SCIENCE CHINA
Technological Sciences

• Article •

December 2014 Vol.57 No.12: 2426–2433
doi: 10.1007/s11431-014-5708-9

Chip formation dependence of machining velocities in nano-scale by molecular dynamics simulations

SU Hao & TANG QiHeng*

State Key Laboratory of Nonlinear Mechanics, Institute of Mechanics, Chinese Academy of Sciences, Beijing 100190, China

Received August 19, 2014; accepted September 20, 2014

In this study, molecular dynamics simulations were carried out to study the effect of machining velocities on the mechanism of chip formation in nano-metric copper. A wide range of cutting velocities was performed from 10 to 2000 m/s, and the microstructure's evolution from a crystalline state to an amorphous state was studied. At the low machining velocity, dislocations were generated from the surface in front of the tool, and the immobile dislocation deduced by the cross slip of dislocation was observed. At the high machining velocity, no crystal dislocation nucleated, but instead disorder atoms were found near the tool. Temperature near the tool region increased with the increasing machining velocities, and the temperature had an important effect on the phase transition of the crystal structure.

molecular dynamics, chip formation, machining velocities, phase transition

Citation: Su H, Tang Q H. Chip formation dependence of machining velocities in nano-scale by molecular dynamics simulations. Sci China Tech Sci, 2014, 57: 2426–2433, doi: 10.1007/s11431-014-5708-9

The current trend towards miniaturization over a wide spectrum of disciplines and industries will continue into the future [1–8]. Therefore, micromechanical machining processes provide an attractive alternative for the production of nano-mesoscale components with high accuracy requirements. However, the development of the micromechanical machining process is limited by a lack of a fundamental understanding of the nature of the deformation mechanism on the atomic scale at the micro-tool/work-piece interface and surface [9,10].

Typically, only several layers of atoms are removed from the surface in the nano-metric machining process, thus rendering experimental studies very difficult to realize. It is uncertain whether or not the conventional continuum machining principles are still valid, due to the small domain size. Therefore, a molecular dynamics (MD) simulation has been adopted to study this process. This is also believed to be a suitable tool to understand the mechanical behavior of the micro-tool/work-piece interface and surface deformation [10].

The MD simulation model has been widely used in the simulation of the machining process since the 1990s. Maekawa and Itoh [10] and Zhang and Tanaka [11] used this method to analyze the friction and the tool wear characteristics. Komanduri et al. [12–15] used it to investigate the effect of tool geometry on the cutting and the thrust forces and the sub-surface deformation. Machining tools with different rake angles [14] and a rounded tool geometry with a different edge radius [15] were utilized. The effect of different interatomic potential on cutting results was studied by Pei et al. [14]. The cutting depth was investigated and believed to have a positive correlation with the cutting force [16–19]. Pei et al. [17] investigated the correlation between the cutting depth and the size effect. The cutting direction and the substrate crystal orientation were found to influence the direction of the generated dislocations [20–22], but all

*Corresponding author (email: qhtang@imech.ac.cn)

the dislocations slipped on the (1 1 1) plane [22].

The machining velocity is very important in the micro-process technique, which is related to the famous Salomon's hypothesis [23] on the macroscopic machining process. However, the previous studies [24–26] concerning about the effect of machining velocities on the tool force and the chip temperature with growing the machined thickness overlooked the effect of the machining velocities on the evolution of micro-structures and chip formation. In the present paper, the MD simulations of orthogonal nano-metric cutting of a single crystal copper are presented. Attention is given to the effect of the machining velocity on the mechanical behavior of the work-piece. A wide range of cutting velocities, from 10 to 2000 m/s, is studied. Finally, the evolution of the microstructures and the different mechanisms of the chip formation are discussed.

1 Computation and modeling

1.1 Interatomic potential

The EAM method has been successful in accurately describing the properties of a metallic system [27–29]. It was evolved from the density-functional theory and the total potential energy for the atomic system is as follows [30]:

$$E_{tot}=\sum_i F_i(\rho_i)+\frac{1}{2}\sum_i\sum_{j(\neq i)}\varphi_{ij}(r_{ij}), \tag{1}$$

where F_i is the embedding function and ρ_i is the local electronic density at the site of the atom i, $\varphi_{ij}(r_{ij})$ represents a pair potential and r_{ij} is the separation between atom i and its neighbor atom j. The EAM potential is used for the interaction between the copper atoms of the work-piece and all the parameters can be found in ref. [31].

The tool material is diamond (carbon, C). The interaction between Cu atoms and C atoms is modeled by the Morse potential [32]:

$$E_i=\sum_{i\neq j}D_0\left[e^{-2\sigma(r_{ij}-r_0)}-2e^{-\sigma(r_{ij}-r_0)}\right], \tag{2}$$

where D_0 denotes the depth of the potential well, σ represents the stiffness parameter, and r_0 is the equilibrium distance between atoms i and j. The parameters for C-Cu interaction are from ref. [11].

Since the stiffness of diamond is much higher than that of Cu, the tool is thereby a rigid body during the MD simulation.

1.2 Cutting model

The orthogonal cutting model for the MD simulation is adopted in this paper, and the schematic is shown in Figure 1. The simulation system is composed of a single crystal of copper and the diamond tool. The sample size is $80a_0\times 60a_0\times 4a_0$, about 78000 atoms, and the tool size is $50a_0\times 50a_0\times 4a_0$, about 72000 atoms, and a_0 is the crystal constant of copper (3.615Å). A periodic boundary condition is applied along z direction to eliminate the effect of free surface [15]. In addition, eight layers of the left and the bottom edges are fixed, and eight layers next to them are a thermostat region which surrounds the Newtonian atoms. The thermostat region serves as a heat reservoir at a constant temperature 300 K to the Newtonian atoms [26]. The Newtonian atoms have an initial velocity distribution of 300 K and are only conducted by Newton's second law thereafter. The rigid tool has a rake angle of α=20° and the clearance angle is set to zero. The angles are unchanged during the machining process.

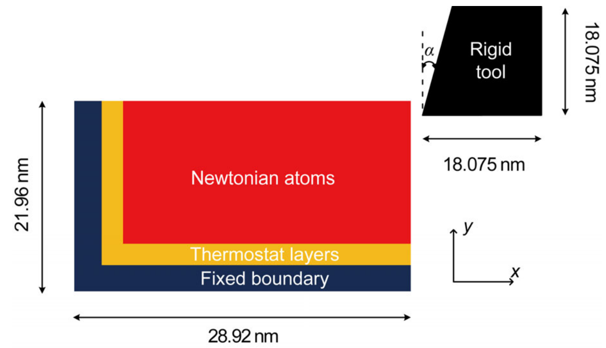

Figure 1 (Color online) Schematic of the nano-metric cutting model.

The machining motion is performed on the (0 1 0) plane of the copper work-piece and the machining direction is along [−1 0 0]. The machining depth is set to 1 nm to ensure that the machining region is only a small portion of the Newtonian area. Based on several testing simulations in different sizes of the work-piece, the dimensions of the work-piece are constructed sufficiently large enough to eliminate the boundary effects, which is similar to that of the system adopted by Fang et al. [33].

2 Results and discussion

2.1 Conventional high cutting speed

Figure 2(a) shows the snapshot of the nano-metric machining process at a machining velocity of 54.225 m/s and the machining distance L is about 1.6 nm. The dashed yellow line represents the cutting plane. The common neighbor analysis (CNA) technique is adopted [34–36], red for the perfect FCC atoms, green for the HCP atoms, and blue for the disorderly (or amorphous) atoms. Two adjacent green lines represent a stacking fault [37]. As shown in Figure 2(a), during the machining process, the surface serves as a dislocation source. The dislocations emitted from the surface slip into the specimen. Previous research [38,39] has

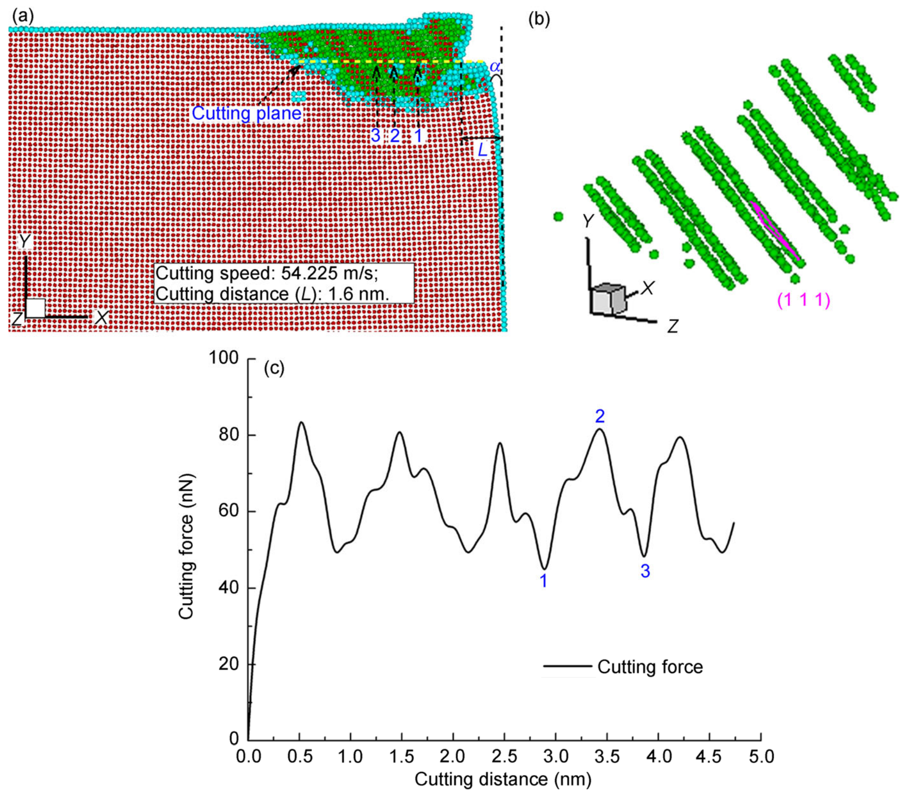

Figure 2 (Color online) Nano-metric material removal process at the machining velocity of 54.225 m/s: (a) Atomic configurations at the cutting distance of 1.6 nm; (b) dislocation slip on the (1 1 1) plane; (c) cutting force acting on the diamond tool.

verified the evidence of dislocations emitted from the surface. Figure 2(b) shows that all of the dislocations are slipping on the (1 1 1) plane, which follows the behavior of the dislocation slip [22,40].

As the tool is driven along the [−1 0 0] direction, the chip forms by splitting from the substrate. Some dislocations are in the chip while others are in the substrate and are multiplying continuously. Figure 2(c) shows the typical curve of the cutting force as the tool is driven forward. Previous research [19,25,26] has attributed the fluctuation of the curve to the MD method itself; however, our simulation results show that as long as the tool meets the dislocations, the curve always tends upward. Points 1, 2, 3 in Figure 2(c) correspond to points 1, 2, 3 in Figure 2(a). From point 1 to 2, the tool cuts the HCP atom's region, and from point 2 to 3, the tool cuts perfectly in the FCC atom's region. It is thereby understood that the FCC crystal has a structure of a smaller planar density than that of the HCP on the cutting plane (0 1 0). Therefore, it is easier to cut from point 2 to 3, and the machining force decreases from its maximum point when the tool crosses point 2. Continuous cutting of the FCC and the HCP atoms leads to the fluctuation of the cutting force.

Figure 3(a) shows the snapshot of the nano-metric machining process with the machining velocity of 90.375 m/s, and the machining distance L is 10.5 nm. The evolution of the atomic structure is observed in regions A, B and C near the tool. An original single crystal is divided into the four regions of A, B, C and D, and due to the dislocations slip, the amorphous atoms move and the crystal rotates. Between grain A and B, there is a "Z" boundary constructed by the disorder atoms which hinders dislocation slipping from A to B. Grain B and C build a twin boundary which is contributed to by the emitted dislocations from the surface and the rotation of the work-piece. The rotation of grain C is due to the shear stress given by the tool. In previous intensive studies of twin deformation, it was revealed that the nano-crystalline containing the twin structure is of a high strength and a good ductility [41], and that the twin structure is stable during extension and shear deformation [42].

In region B, the phenomenon of cross slip and the formation of Lomer-Cottrell (LC) locks are observed. This is displayed as a yellow rectangle, and zooms out in Figure 3(a), and also in the schematic of the dislocation evolution in Figure 3(b). The partial dislocation $E\gamma(\frac{1}{6}[1\bar{2}\bar{1}]/(11\bar{1}))$ slips on the $(11\bar{1})$ plane. First a cross slip occurs, i.e. $E\gamma\rightarrow E\beta+\beta\gamma$.

$$\frac{1}{6}[1\bar{2}\bar{1}]\rightarrow\frac{1}{6}[1\bar{1}\bar{2}]+\frac{1}{6}[0\bar{1}1],$$

where the stair-rod dislocation $\beta\gamma=\frac{1}{6}[0\bar{1}1]$ is an immovable LC lock, and the first cross slip is completed. Then the partial dislocation $E\beta=\frac{1}{6}[1\bar{1}\bar{2}]$ on the $(1\bar{1}1)$ expe-

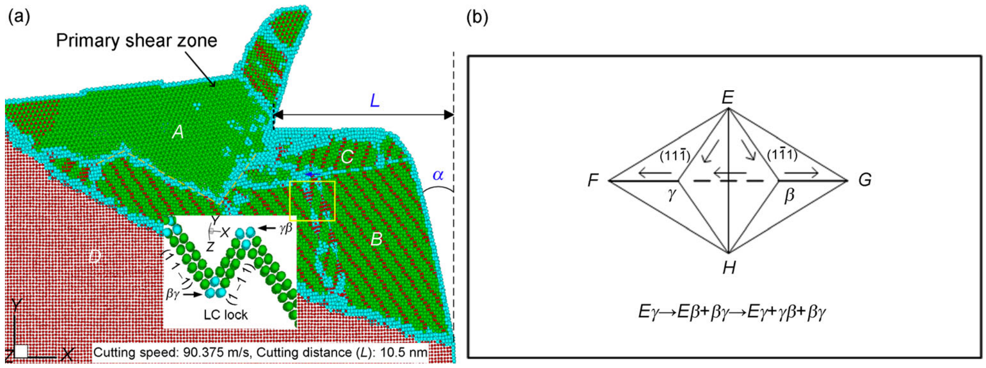

Figure 3 (Color online) Nano-metric material removal process at the machining velocity of 90.375 m/s: (a) Atomic configurations of the immobile dislocation at the cutting distance of 10.5 nm; (b) schematic of the cross slip of dislocation.

riences the second cross slip: $E\beta \rightarrow E\gamma + \gamma\beta$.

$$\frac{1}{6}[1\bar{1}\bar{2}] \rightarrow \frac{1}{6}[1\bar{2}\bar{1}] + \frac{1}{6}[01\bar{1}],$$

where $\gamma\beta = \frac{1}{6}[01\bar{1}]$ is also an immovable LC lock, and the second cross slip is completed. The partial dislocation $E\gamma$ slips along the $(11\bar{1})$ plane and is assimilated by the interface. Two stair-rod dislocations $\beta\gamma$ and $\gamma\beta$ remain in region *B*. Due to the stair-rod dislocation (LC lock) being located on the (1 0 0) plane, it is difficult to move, resulting in the materials' consolidation [43].

2.2 Ultrahigh cutting speed

Figure 4(a) illustrates an ultrahigh machining velocity of 180.75 m/s over a distance of 10.5 nm. A comparison of the rotated angle of the right boundary of the simulation sample is made at the different machining velocities. The rotated angle of right boundary shown in Figure 4(a) is smaller than that in both Figures 2(a) and 3(a). This may be attributed to the friction of the interface between the work-piece and the tool rake face. It is deduced that the friction at the tool work-piece interface decreases with the increase of machining velocities based on our simulation. This is verified by ref. [25]. Due to the increase of machining velocity, the temperature in the interface region between the tool and the work-piece also increases which leads to a reduction of the friction force and to the thermal softening of the work-piece. Figure 4(b) shows the curve of temperature near the tool regions *S*1 and *S*2 versus the machining distance at three different machining velocities. The local temperatures are about 450 K at a conventional machining velocity and 600 K at an ultrahigh machining velocity, respectively. Temperature *T* is computed based on eqs. (3) and (4) as shown below:

$$\frac{3}{2}(N_1+N_2)K_B T = \frac{1}{2}\sum_i^{N_1} m_i \| v_i - \overline{v_1} \|^2 + \frac{1}{2}\sum_i^{N_2} m_i \| v_i - \overline{v_2} \|^2, \quad (3)$$

$$\overline{v_j} = \frac{1}{N_j}\sum_i^{N_j} v_i, (j = 1, 2), \quad (4)$$

where N_1 and N_2 represent the number of atoms in the local regions near the tool as shown in Figure 4. The local region is about 4 layers of atoms along the y direction, v_i is the velocity of atom *i* and K_B is the Boltzmann constant.

The atoms in regions *S*1 and *S*2 slip along with the machining tool and the high temperature is generated due to the friction between the work-piece and the machining tool. Porter and Eastering [44] pointed out that the transformation temperature decreased with increasing pressure as the phase of perfect metal structure transformed into the disorder phase. As it is noted that disorder atoms appear in regions *S*1 and *S*2, this is attributed to the acting of pressure, temperature and the atoms slipping along the tool. Similarly, the amorphous atoms are easily generated in the primary shear zone. Figure 4(a) shows that the formed chip is composed of both perfect FCC atoms and amorphous atoms. Some amorphous atoms appear in the primary shear zone and maintain their disorder states in the region of the chip. These amorphous atoms continue to move against the tool rake face which adds energy and force and causes the amorphous atoms to reach a high temperature. However, other atoms recover their original crystal state to some extent as soon as they move out of tool rake face. The atoms can relax as they are at a lower temperature. The simulation results are similar to those shown in ref. [26].

Observation reveals that no dislocations exist in the substrate after machining 10.5 nm. The disorder atoms in the primary shear zone and regions *S*1 and *S*2 do not recover to a crystal state because the machining velocity is ultrahigh, the temperature in the region near the tool reaches 420 K and the temperature is maintained during the machining process. Figure 4(c) indicates the temperature variation of the region near the tool.

2.3 Impact cutting speed

Figures 5(a)–(c) show the snapshots of the nano-metric

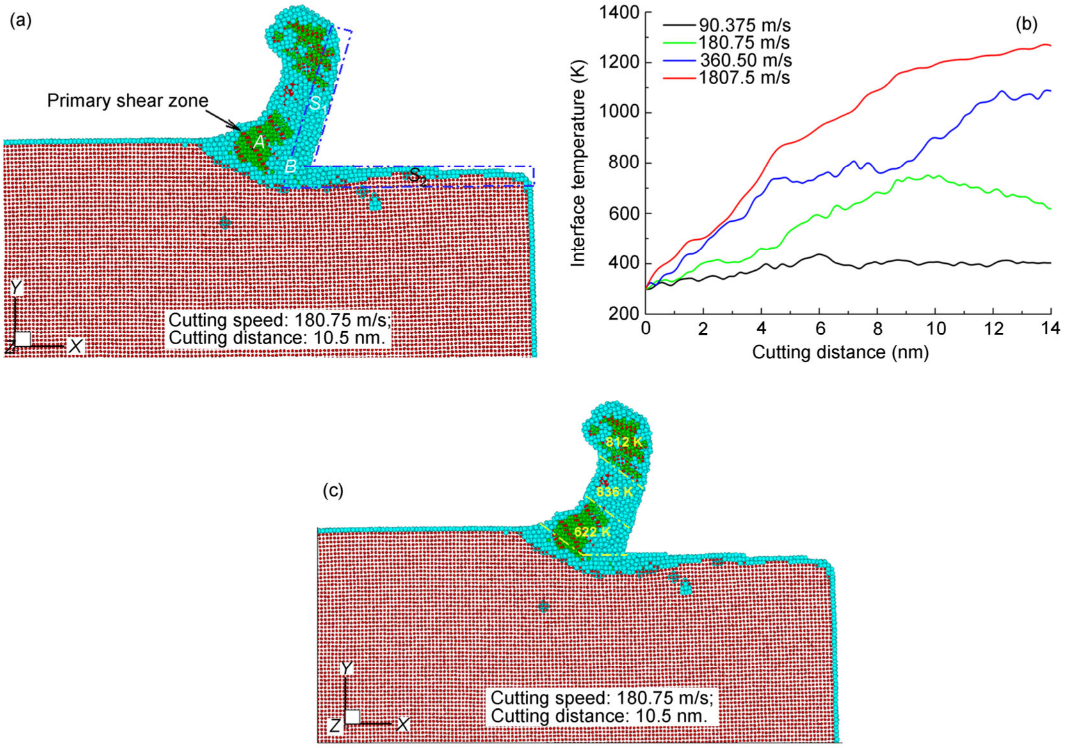

Figure 4 (Color online) (a) Snapshot of the nano-metric material removal process at the machining velocity of 180.75 m/s and the machining distance of 10.5 nm; (b) interface temperature for the different machining velocities; (c) temperature variation in the chip as shown in (a).

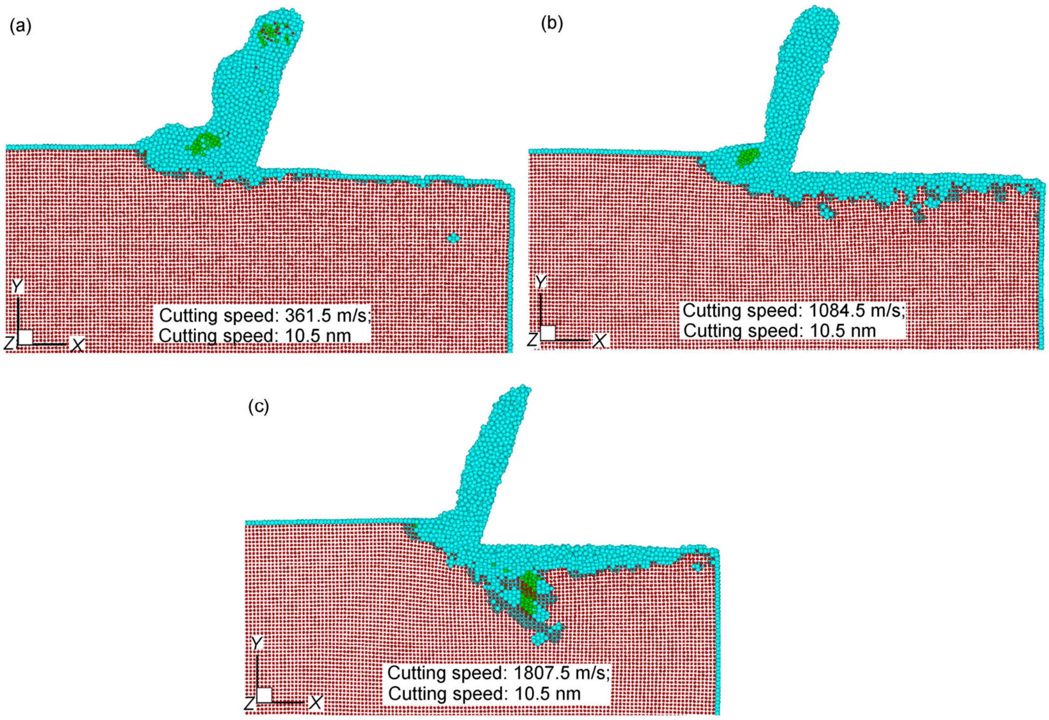

Figure 5 (Color online) Snapshots of nano-metric material removal process for different machining velocities: (a) 361.5 m/s; (b) 1084.5 m/s; (c) 1807.5 m/s.

machining results at the machining velocities of 361.5, 1084.5 and 1807.5 m/s, respectively. The machining distances are at about 10.5 nm which is the same as that of the ultrahigh machining. A difference is shown here from Figure 4(a) that crystal and amorphous atoms are merged together at the beginning of the chip formation. The machining velocity is now 361.5 m/s and there are some HCP atoms left in the end of the chip. Most of the atoms in the chip are in the disorder state. As the machining velocity increases, the temperature in the region near the tool increases. The HCP atoms decrease and transform into disorder atoms due to the high temperature. The result of moving the machining velocity up to 1807.5 m/s is that the HCP atoms are no longer observed in the chip. The results can be observed in Figures 5(b) and (c). The simulation results at the impact machining velocity are clearly different from those of the ultrahigh machining velocity [26]. This may be attributed to the high temperature caused by friction between the tool and the work-piece. The maximum temperature reached is 1250 K as shown in Figure 4(b).

As the machining is performed, the phase transformation occurs in the local region near the tool and a lot of the FCC atoms transform into HCP and disorder atoms. The curves of the statistical results of the HCP and disorder atoms versus the machining distances at different machining velocities are shown in Figure 6. The HCP and the disorder atoms increase not only with the machining distance but also with temperature. Therefore, the effect of temperature on mechanical behavior of work-pieces is significant. The strength of the original crystal lattice decreases due to the raised temperature and the disorder atoms near the tool prevent dislocation nucleated.

In order to reveal the deformation state of the chip at the different temperatures, a comparison of potential energy is carried out. Figure 7(a) indicates the curve of the potential energy versus strain for the perfect FCC crystal of copper at the absolute 0 K. The potential energy of the atoms in the chip is shown in Figure 7(b). This potential energy of the atoms in the chip increases with the increasing of the machining velocities. Figure 7(a) illustrates the potential energy of perfect crystal copper versus deformation and Figure 7(b) shows the curve of potential energy versus the machining velocities. As the machining velocities are 361.5, 1084.5 and 1807.5 m/s, the potential energies are −3.25, −3.13 and −2.95 eV, respectively. This is corresponding to the compression deformation of −5%, −7% and −10%. According to experiment [45] and theoretical calculation [46], the contribution of thermal expansion to the total deformation is small in our simulation. For example, as the machining velocity is 1807.5 m/s, the average temperature of the chip is about 1250 K and the corresponding thermal strain is about 1.3%, which is far less than the compressive strain 10%. Therefore, the effect of temperature on the average potential energy is limited and it does not affect our theoretical analysis.

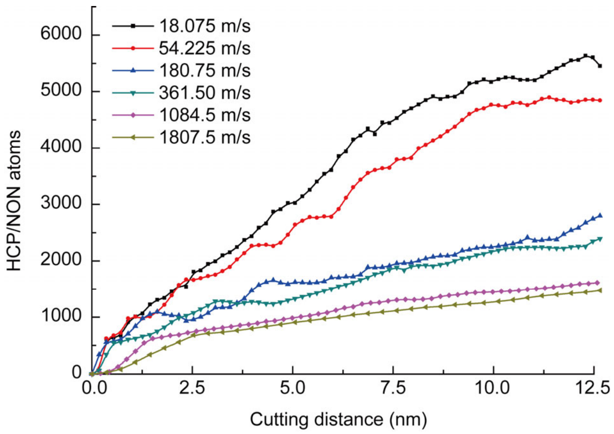

Figure 6 (Color online) Total number of phase transition atoms for different machining velocities.

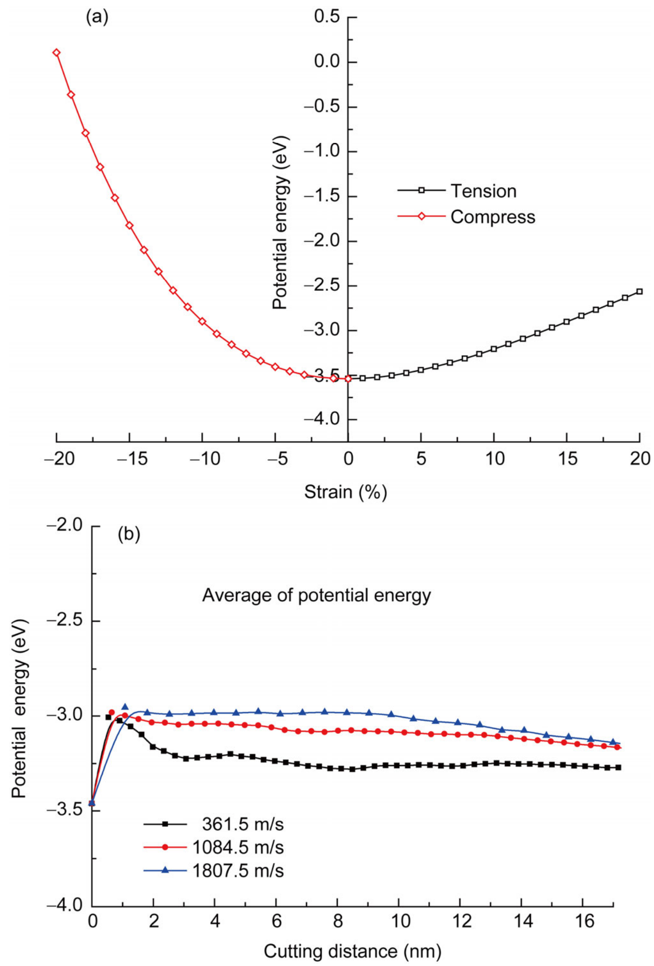

Figure 7 (Color online) Average atom potential energy of a single crystal copper under different conditions. (a) tension/compress; (b) different machining velocities.

3 Conclusions

In this study, the effect of machining velocities on the chip formation by using the MD simulations is explored. Studies on the conventional machining velocity, the ultrahigh machining velocity and the impact machining velocity are carried out. Some conclusions are as follows.

The effect of the machining velocities on temperature, pressure and the transition of metal structure is analyzed. The temperature in the local region near the tool is closely related to the machining velocities and the use of the different machining velocities leads to the different deformation behaviors in the chips.

The potential energy analysis is carried out to reveal the deformation behavior of the chips. The strain of compression deformation increases with the machining velocities.

The Lomer-Cottrell lock deduced by the cross slip is observed and the immobile dislocations may consolidate the work-piece.

The research was supported by the National Natural Science Foundation of China (Grant Nos. 11132011, 11021262 and 11172303), and the National Basic Research Program of China ("973" Project) (Grant No. 2012CB937500).

1 Du M, Ma Z S, Ye X Y, et al. On-chip fast mixing by a rotary peristaltic micropump with a single structural layer. Sci China Tech Sci, 2013, 56: 1047–1054

2 Wang B B, Wang F C, Zhao Y P. Understanding formation mechanism of ZnO diatomic chain and multi-shell structure using physical mechanics: Molecular dynamics and first-principle simulations? Sci China-Phys Mech Astron, 2012, 55: 1138–1146

3 Yao Y, Huang Z X. Investigation on coaxial stability of nano-bearing under two axis-deviation perturbations. Sci China-Phys Mech Astron, 2010, 53: 2274–2283

4 Deng Y C, Quan Z H, Zhao Y H, et al. Experimental investigations on the heat transfer characteristics of micro heat pipe array applied to flat plate solar collector. Sci China Tech Sci, 2013, 56: 1177–1185

5 Shang Y F, Ye X Y, Feng J Y. Theoretical analysis and simulation of thermoelastic deformation of bimorph microbeams. Sci China Tech Sci, 2013, 56: 1715–1722

6 Li H F, Jia R, Dou B F, et al. Research on ultra-small textured surface of multicrystalline silicon solar cell. Sci China Tech Sci, 2013, 56: 952–956

7 Chan K T, Zhao Y P. The dispersion characteristics of the waves propagating in a spinning single-walled carbon nanotube. Sci China-Phys Mech Astron, 2011, 54: 1854–1865

8 Xu K, Tian X J, Wu C D, et al. Fabrication of single-walled carbon nanotube-based highly sensitive gas sensors. Sci China Tech Sci, 2013, 56: 32–35

9 Kim C J, Mayor R, Ni J. Molecular dynamics simulations of plastic material deformation in machining with a round cutting edge. Int J Precis Eng Man, 2012, 13: 1303–1309

10 Maekawa K, Itoh A. Friction and tool wear in nano-scale machining-a molecular-dynamics approach. Wear, 1995, 188: 115–122

11 Zhang L C, Tanaka H. Towards a deeper understanding of wear and friction on the atomic scale-a molecular dynamics analysis. Wear, 1997, 211: 44–53

12 Komanduri R, Chandrasekaran N, Raff L M. MD simulation of exit failure in nanometric cutting. Mat Sci Eng A-Struct, 2001, 311: 1–12

13 Promyoo R, El-Mounayri H, Yang X P. Molecular dynamics simulation of nanometric cutting. Mach Sci Technol, 2010, 14: 423–439

14 Pei Q X, Lu C, Fang F Z, et al. Nanometric cutting of copper: A molecular dynamics study. Comp Mater Sci, 2006, 37: 434–441

15 Hosseini S V, Vahdati M. Modeling the effect of tool edge radius on contact zone in nanomachining. Comp Mater Sci, 2012, 65: 29–36

16 Chen J X, Liang Y C, Bai Q S, et al. Researching nanometric cutting of copper based on molecular dynamics. J Comput Theor Nanos, 2008, 5: 1485–1489

17 Pei Q X, Lu C, Lee H P, et al. Study of materials deformation in nanometric cutting by large-scale molecular dynamics simulations. Nanoscale Res Lett, 2009, 4: 444–451

18 Fang T H, Weng C I. Three-dimensional molecular dynamics analysis of processing using a pin tool on the atomic scale. Nanotechnology, 2000, 11: 148–153

19 Shi J, Shi Y X, Liu C R. Evaluation of a three-dimensional single-point turning at atomistic level by a molecular dynamic simulation. Int J Adv Manuf Tech, 2011, 54: 161–171

20 Pen H M, Liang Y C, Luo X C, et al. Multiscale simulation of nanometric cutting of single crystal copper and its experimental validation. Comp Mater Sci, 2011, 50: 3431–3441

21 Komanduri R, Chandrasekaran N, Raff L M. Md simulation of nanometric cutting of single crystal aluminum-effect of crystal orientation and direction of cutting. Wear, 2000, 242: 60-88

22 Chen M J, Xiao G B, Lu L H, et al. Mechanism of chip-formation in nanometric cutting of single-crystal copper by molecular dynamics. J Comput Theor Nanos, 2012, 9: 110–116

23 Longbottom J M, Lanham J D. A review of research related to salomon's hypothesis on cutting speeds and temperatures. Int J Mach Tool Manu, 2006, 46: 1740–1747

24 Ye Y Y, Biswas R, Morris J R, et al. Molecular dynamics simulation of nanoscale machining of copper. Nanotechnology, 2003, 14: 390–396

25 Romero P A, Anciaux G, Molinari A, et al. Friction at the tool-chip interface during orthogonal nanometric machining. Model Simul Mater Sci, 2012, 20:

26 Romero P A, Anciaux G, Molinari A, et al. Insights into the thermo-mechanics of orthogonal nanometric machining. Comp Mater Sci, 2013, 72: 116–126

27 Yuan F P. Atomistic simulation study of tensile deformation in bulk nanocrystalline bcc iron. Sci China-Phys Mech Astron, 2012, 55: 1657–1663

28 Liu X M, Yang X B, Wei Y G. Yielding behavior of copper nanowire in the presence of vacancies. Sci China-Phys Mech Astron, 2012, 55: 1010–1017

29 Lin E Q, Niu L S, Shi H J, et al. Molecular dynamics study on the nano-void growth and coalescence at grain boundary. Sci China-Phys Mech Astron, 2012, 55: 86–93

30 Daw M S, Baskes M I. Embedded-atom method-derivation and application to impurities, surfaces, and other defects in metals. Phys Rev B, 1984, 29: 6443–6453

31 Foiles S M, Baskes M I, Daw M S. Embedded-atom-method functions for the fcc metals Cu, Ag, Au, Ni, Pd, Pt, and their alloys. Phys Rev B, 1986, 33: 7983–7991

32 Morse P M. Diatomic molecules according to the wave mechanics. Ii. Vibrational levels. Phys Rev, 1929, 34: 57–64

33 Fang T H, Weng C I, Chang J G. Molecular dynamics simulation of nano-lithography process using atomic force microscopy. Surf Sci, 2002, 501: 138–147

34 Faken D, Jónsson H. Systematic analysis of local atomic structure combined with 3 d computer graphics. Comp Mater Sci, 1994, 2: 279–286

35 Tsuzuki H, Branicio P S, Rino J P. Structural characterization of deformed crystals by analysis of common atomic neighborhood. Comput Phys Commun, 2007, 177: 518–523

36 An M, Song H. Atomic simulations of influence of twinning on crack propagation of Al?. Sci China-Phys Mech Astron, 2013, 56: 1938–1944

37 Yamakov V, Wolf D, Phillpot S R, et al. Dislocation processes in the deformation of nanocrystalline aluminium by molecular-dynamics simulation. Nat Mater, 2002, 1: 45–48

38 Diao J K, Gall K, Dunn M L, et al. Atomistic simulations of the yielding of gold nanowires. Acta Mater, 2006, 54: 643–653

39 Tang Q H. Effect of size on mechanical behavior of au pillars by molecular dynamics study. Sci China-Phys Mech Astron, 2012, 55: 1111–1117

40 Yang Z, Jiao F, Lu Z, et al. Coupling effects of stress and ion irradiation on the mechanical behaviors of copper nanowires. Sci China-Phys Mech Astron, 2013, 56: 498–505

41 Hodge A M, Furnish T A, Shute C J, et al. Twin stability in highly nanotwinned cu under compression, torsion and tension. Scripta Mater, 2012, 66: 872–877

42 Su H, Tang Q H. MD simulations of loading rate dependence of detwinning deformation in nanocrystalline Ni. Sci China-Phys Mech Astron, 2013, 56: 491–497

43 Lee J H, Holland T B, Mukherjee A K, et al. Direct observation of lomer-cottrell locks during strain hardening in nanocrystalline nickel by *in situ* tem. Sci Rep, 2013, 3:1061–1066

44 Porter D A, Easterling K E. Phase Transformations in Metals and Alloys. London: Van Nostrand Reinhold, 1981

45 Billings B H, Cray D E. American Institute of Physics Handbook. Michigan: McGraw-Hill, 1972

46 Liu X L, Tang Q H, Wang T C. A continuum thermal stress theory for crystals based on interatomic potentials. Sci China-Phys Mech Astron, 2014, 57: 208–217